

The power of  $J_{1q} + J_{2q}$  can be obtained through direct calculations.

$$\begin{aligned}
 E \{ |J_{1q}|^2 \} &= E_{s,h,\phi} \left\{ \frac{1}{N^2} \sum_{l_1=0}^{N-1} \sum_{k_1=0}^{N-1} \sum_{n_1=0}^{N-1} s_{n_1} e^{j \frac{2\pi k_1 n_1}{N}} \right. \\
 &\quad \times h_{l_1-k_1} \phi_{l_1} e^{-j \frac{2\pi l_1 (q+\Delta q)}{N}} \\
 &\quad \left. \times \sum_{l_2=0}^{N-1} \sum_{k_2=0}^{N-1} \sum_{n_2=0}^{N-1} s_{n_2}^* e^{-j \frac{2\pi k_2 n_2}{N}} h_{l_2-k_2} \phi_{l_2} e^{j \frac{2\pi l_2 (q+\Delta q)}{N}} \right\} \\
 &= \frac{\sigma_\phi^2}{N} \sum_{k=0}^{N-1} \sum_{l=k}^{\min(k+V-1, N-1)} \sigma_{h,l-k}^2. \quad (28)
 \end{aligned}$$

Similarly

$$E \{ |J_{2q}|^2 \} = \frac{\sigma_\phi^2}{N} \sum_{k=0}^{N-1} \sum_{l=0}^{k-N+V-1} \sigma_{h,l+N-k}^2. \quad (29)$$

Due to the independence assumption on different paths, it is straightforward to check also that

$$E \{ J_{1q} J_{2q}^* \} = E \{ J_{1q}^* J_{2q} \} = 0. \quad (30)$$

## REFERENCES

- [1] "First report and order, revision of Part 15 of the commission's rules regarding ultra-wideband transmission systems," FCC, ET Docket 98-153, Feb. 14, 2002.
- [2] —, "Design of a multiband OFDM system for realistic UWB channel environments," *IEEE Trans. Microw. Theory Tech.*, vol. 52, pp. 2123-2138, Sep. 2004.
- [3] A. Batra, Multi-band OFDM physical layer proposal for IEEE 802.15 Task Group 3a IEEE P802.15-04/0493r1, Sep. 2004.
- [4] A. Bahai, B. Saltzberg, and M. Ergen, *Multi-Carrier Digital Communications: Theory and Applications of OFDM*. New York: Kluwer, 2004.
- [5] B. Muquet, "Cyclic prefixing or zero padding for wireless multicarrier transmissions?," *IEEE Trans. Commun.*, vol. 50, pp. 2136-2148, Dec. 2002.
- [6] C. R. Athaudage, "BER sensitivity of OFDM systems to time synchronization error," in *Proc. 8th Int. Conf. Communication Systems (ICCS)*, Nov. 2002, vol. 1, pp. 42-46, 2002.
- [7] Y. Mostofi and D. C. Cox, "Analysis of the effect of timing synchronization errors on pilot-aided OFDM systems," in *Proc. 37th Asilomar Conf. Signals, Systems, Computers*, Nov. 2003, vol. 1, pp. 638-642.
- [8] Y. Zhao and S. G. Haggman, "Sensitivity to Doppler shift and carrier frequency errors in OFDM systems-the consequences and solutions," in *Proc. IEEE 46th Vehicular Technology Conf. (VTC)*, Apr. 1996, vol. 3, pp. 1564-1568.
- [9] X. Wang, T. T. Tjhung, Y. Wu, and B. Caron, "SER performance evaluation and optimization of OFDM system with residual frequency and timing offsets from imperfect synchronization," *IEEE Trans. Broadcast.*, vol. 49, no. 2, pp. 170-177, Jun. 2003.
- [10] A. Saleh and R. Valenzuela, "A statistical model for indoor multipath propagation," *IEEE J. Sel. Areas Commun.*, vol. SAC-5, pp. 128-137, Feb. 1987.
- [11] J. Foerster, "Channel Modeling Sub-Committee Report Final," IEEE P802.15-02/368r5-SG3a, Dec. 2002.

## New Approaches for Chirplet Approximation

J. M. Greenberg, Zhisong Wang, and Jian Li

**Abstract**—This correspondence proposes efficient algorithms for approximating complex-valued and real-valued signals as a weighted sum of multiple chirplet atoms, which are characterized by four parameters, namely the scale, time, frequency, and chirp rate. Direct sequential estimation of the parameters of multiple chirplets causes error propagations, i.e., the estimated parameters of the initial chirplets significantly affect the parameter estimation of the subsequent chirplets and may result in large chirplet approximation errors. To deal with this problem, we further exploit a relaxation (RELAX) method for recursive chirplet parameter estimation. RELAX can be used in conjunction with time-domain or frequency-domain algorithms to improve the parameter estimation accuracy for multiple chirplets. Unlike previous methods, our chirplet approximations require neither any *a priori* complete dictionary of chirplets nor complicated multidimensional searches to obtain suitable choices of chirplet parameters. The effectiveness of the proposed approaches is demonstrated via a number of simulated examples.

**Index Terms**—Atomic decomposition, chirplets, matching pursuit, relaxation method, time-frequency analysis, Wigner-Ville distribution.

## I. INTRODUCTION

In the last decade, a lot has been written about how to approximate a given complex-valued signal

$$P(t) = a(t) \exp(-j\phi(t)), \quad a(t) \geq 0 \quad (1)$$

by  $K$  chirplets; that is, how to find parameters  $C_k \in C$ ,  $\sigma_k > 0$ , and real-valued numbers  $t_k$ ,  $\omega_k$ , and  $c_k$  so that

$$\begin{aligned}
 a(t) \exp(-j\phi(t)) &\simeq \sum_{k=0}^{K-1} \frac{C_k}{(\pi\sigma_k)^{1/4}} \\
 &\times \exp \left[ -\frac{(t-t_k)^2}{2\sigma_k} - j \left( \omega_k(t-t_k) + \frac{c_k(t-t_k)^2}{2} \right) \right]. \quad (2)
 \end{aligned}$$

The parameters need to be chosen so that the two functions appearing in (2) are close in some prescribed sense. It should be noted that the functions

$$\begin{aligned}
 g(t-t_k; \sigma_k, \omega_k, c_k) &\stackrel{\text{def}}{=} \frac{1}{(\pi\sigma_k)^{1/4}} \\
 &\cdot \exp \left[ -\frac{(t-t_k)^2}{2\sigma_k} - j \left( \omega_k(t-t_k) + \frac{c_k(t-t_k)^2}{2} \right) \right] \quad (3)
 \end{aligned}$$

Manuscript received December 9, 2004; revised April 26, 2006. The associate editor coordinating the review of this manuscript and approving it for publication was Dr. Hongya Ge. This work was supported in part by the National Science Foundation Grants CCR-0104887 and ECS-0097636.

J. M. Greenberg is with Carnegie Mellon University, Pittsburgh, PA 15213 USA (e-mail: greenber@andrew.cmu.edu).

Z. Wang was with the Department of Electrical and Computer Engineering, University of Florida, Gainesville, FL 32611 USA. He is now with the School of Health Information Sciences, University of Texas Health Science Center at Houston, Houston, TX 77030 USA (e-mail: Zhi-Song.Wang@uth.tmc.edu).

J. Li is with the Department of Electrical and Computer Engineering, University of Florida, Gainesville, FL 32611 USA (e-mail: li@dsp.ufl.edu).

Color versions of Figs. 1-5 are available online at <http://ieeexplore.ieee.org>. Digital Object Identifier 10.1109/TSP.2006.885725

are typically referred to as *chirplet atoms* that are characterized by the scale  $\sqrt{\sigma_k}$ , time  $t_k$ , frequency  $\omega_k$  and chirp rate  $c_k$ , and satisfy

$$\begin{aligned} \|g\|^2 &= \langle g, g \rangle \\ &= \int_{-\infty}^{\infty} g(t - t_k; \sigma_k, \omega_k, c_k) \bar{g}(t - t_k; \sigma_k, \omega_k, c_k) dt = 1. \end{aligned} \quad (4)$$

Here,  $\bar{(\cdot)}$  denotes the complex conjugate.

Such four-parameter chirplet approximation offers more efficient representations of the radar, seismic, and biological signals than the representations obtained using short time Fourier transform, Gabor transform, wavelet transform, and wavelet packets. A sampling of the literature on this subject may be found in [1]–[6] and the references contained therein. Applications of chirplet approximation include time-frequency analysis, feature extraction, data compression, and denoising. The central problem in establishing a formula like (2) is the development of an efficient method for obtaining the parameters  $(C_k, \sigma_k, t_k, \omega_k, c_k)$ . The “matching-pursuit” and “ridge-pursuit” algorithms have been used by a number of authors (for details, see [2], [4], and [5]). They may be slow since they require complicated multidimensional searches to obtain chirplet parameter estimates. They also demand an *a priori* complete dictionary of chirplets. In this correspondence, we present new methods for obtaining chirplet approximations for both complex-valued signals and real-valued signals. For a complex-valued signal  $a(t)\exp(-j\phi(t))$ , we propose two time-domain algorithms to deal with functions of the form  $a_k(t)\exp(-j\phi_k(t))$  by using local information about  $a_k(t)$  and  $\phi_k(t)$  in a neighborhood of a point  $t_k$ , which is the location of a global maximum of  $a_k(t)$ . Similarly, we can apply a frequency-domain algorithm to deal with the Fourier transform of the complex-valued signal by using local information in the frequency domain. To save space, this frequency-domain algorithm is not presented in the correspondence. For a real-valued time-domain signal, we can decompose it into chirplets based on its analytic signal using a time-domain algorithm or based on its Fourier transform using a frequency-domain algorithm. Unlike previously proposed methods, our chirplet approximations do not require any *a priori* complete dictionary of chirplets, and we do not have to apply complicated multidimensional searches to obtain suitable choices of chirplet parameters.

## II. CHIRPLET APPROXIMATION FOR COMPLEX-VALUED SIGNALS

For  $k = 0$ , we let the zeroth-order residual  $R_0(t)$  be the original signal; i.e.,

$$R_0(t) = a(t)\exp(-j\phi(t)), \quad a(t) \geq 0 \quad (5)$$

and for any integer  $k \geq 0$  we assume that the  $k$ th residual has the form

$$R_k(t) = a_k(t)\exp(-j\phi_k(t)), \quad (6)$$

where  $a_k(t) \geq 0$  is the amplitude of the residual and  $\phi_k(t)$  is the real-valued phase. We let  $t_k$  be the location of a global maximum of  $a_k(t)$  (what we have in mind is that  $a_k(t)$  has a finite number of local maxima and that the global maximum may be found by a simple search) and we

assume that this maximum is nondegenerate; i.e., that  $a_k^{(2)}(t_k) < 0$ . Here,  $(\cdot)^{(m)}$  denotes the  $m$ th-order derivative. In this situation, we let

$$\sigma_k = \frac{a_k(t_k)}{|a_k^{(2)}(t_k)|}, \quad \phi_k = \phi_k(t_k), \quad \omega_k = \phi_k^{(1)}(t_k), \quad \text{and} \quad c_k = \phi_k^{(2)}(t_k) \quad (7)$$

and define the  $(k + 1)$ th residual by

$$\begin{aligned} R_{k+1}(t) &= R_k(t) - (\pi\sigma_k)^{1/4} a_k(t_k) \exp(-j\phi_k) g(t - t_k; \sigma_k, \omega_k, c_k). \end{aligned} \quad (8)$$

Taylor’s Theorem implies that for  $t$  near to  $t_k$ ,  $R_{k+1}(t) = O((t - t_k)^3)$  and thus if we write  $R_{k+1}(t)$  as

$$R_{k+1}(t) = a_{k+1}(t)\exp(-j\phi_{k+1}(t)) \quad (9)$$

the global maximum of  $a_{k+1}(t)$  is unlikely to occur near  $t_k$  but if it does, we are guaranteed that the  $(k + 1)$ th residual is uniformly small. One could easily envision using a greedy version of the above algorithm where, instead of using only the global maximum at the  $k$ th stage, one also uses some or all of the local maxima of  $a_k(t)$ , namely, the numbers  $t_{k,1} < t_{k,2} < \dots < t_{k,N(k)}$ .

An alternative algorithm is to choose the parameters  $(t_k, \omega_k, c_k)$  as we did in (7) but to instead write the  $(k + 1)$ th residual as

$$\begin{aligned} R_{k+1}(t) &= R_k(t) - \left( \int_{-\infty}^{\infty} R_k(s) \bar{g}(s - t_k; \sigma_k, \omega_k, c_k) ds \right) \\ &\quad \cdot g(t - t_k; \sigma_k, \omega_k, c_k) \end{aligned} \quad (10)$$

where  $\sigma_k > 0$  is chosen to maximize

$$\mu_k(\sigma_k) = \left| \int_{-\infty}^{\infty} R_k(s) \bar{g}(s - t_k; \sigma_k, \omega_k, c_k) ds \right|. \quad (11)$$

We note that if the original signal  $F(t) = R_0(t)$  is in  $L_1 \cap L_2$ , where  $L_p$  denotes a space composed of the measurable functions  $f(t)$  for which  $\left( \int_{-\infty}^{\infty} |f(t)|^p dt \right)^{1/p} < \infty$ , then the same will be true of each of the residuals  $R_k(t)$ . This guarantees that the numbers  $\mu_k(\sigma_k)$  defined in (11) satisfy two properties. First, when  $\sigma_k$  goes towards  $0^+$ ,  $\mu_k(\sigma_k)$  is asymptotic to  $2^{1/2}(\pi\sigma_k)^{1/4} a_k(t_k)$ . Second, when  $\sigma_k$  goes towards  $\infty$ ,  $\mu_k(\sigma_k)$  is less than or equal to  $\int_{-\infty}^{\infty} a_k(s) ds / (\pi\sigma_k)^{1/4}$ . This follows from (after substituting (3) and (6) into (11))

$$\begin{aligned} \mu_k(\sigma_k) &\leq \int_{-\infty}^{\infty} a_k(s) \frac{1}{(\pi\sigma_k)^{1/4}} \exp\left[-\frac{(s - t_k)^2}{2\sigma_k}\right] ds \\ &\leq 2^{1/2}(\pi\sigma_k)^{1/4} \\ &\quad \cdot \int_{-\infty}^{\infty} a_k(s) \frac{1}{(2\pi\sigma_k)^{1/2}} \exp\left[-\frac{(s - t_k)^2}{2\sigma_k}\right] ds \end{aligned} \quad (12)$$

and

$$\int_{-\infty}^{\infty} \frac{1}{(2\pi\sigma_k)^{1/2}} \exp\left[-\frac{(s - t_k)^2}{2\sigma_k}\right] ds = 1. \quad (13)$$

Thus, there is a point  $\sigma_k^* < \infty$  such that  $\mu_k(\sigma_k)$  attains its global maximum. With this alternative algorithm, we choose  $\sigma_k = \sigma_k^*$ . We no longer have the pointwise estimate  $R_{k+1}(t) = O((t - t_k)^3)$  but we do have

$$\|R_{k+1}\|_2^2 = \|R_k\|_2^2 - \mu_k^2(\sigma_k). \quad (14)$$

Thus, our alternative algorithm is norm reducing in  $L_2$  with  $\mu_k(\sigma_k)$  as large as possible.

Our algorithms are different from the ‘‘matching-pursuit’’ type algorithms [2], [4]. There, one attempts to pick parameters  $t_k$ ,  $\sigma_k$ ,  $\omega_k$ , and  $c_k$  so that

$$F(t_k, \sigma_k, \omega_k, c_k) \stackrel{\text{def}}{=} |\langle R_k(t), g(t - t_k, \sigma_k, \omega_k, c_k) \rangle| \\ \equiv \left| \int_{-\infty}^{\infty} R_k(t) \bar{g}(t - t_k, \sigma_k, \omega_k, c_k) dt \right| \quad (15)$$

is a maximum. Typically, this involves a complicated four-dimensional search procedure. Once the parameters  $(t_k, \sigma_k, \omega_k, c_k)$  have been determined, the  $(k + 1)$ th residual is defined by

$$R_{k+1}(t) = R_k(t) - \langle R_k(t), g(t - t_k, \sigma_k, \omega_k, c_k) \rangle g(t - t_k, \sigma_k, \omega_k, c_k) \quad (16)$$

and the residual satisfies

$$\|R_{k+1}\|_2^2 = \|R_k\|_2^2 - |\langle R_k(t), g(t - t_k, \sigma_k, \omega_k, c_k) \rangle|^2. \quad (17)$$

### III. CHIRPLET APPROXIMATION FOR REAL-VALUED SIGNALS

In Section II, we dealt with chirplet approximations for a complex-valued signal, while in this section, we focus on chirplet approximation for a real-valued signal  $f(t)$ , whose Fourier transform

$$f(\omega) \stackrel{\text{def}}{=} \int_{-\infty}^{\infty} \exp(-j\omega t) f(t) dt \quad (18)$$

satisfies

$$\bar{f}(\omega) = f(-\omega). \quad (19)$$

The identity in (19) guarantees that if we write  $f(\omega)$  as

$$f(\omega) = A_0(\omega) \exp(-j\psi_0(\omega)) \quad (20)$$

where  $A_0(\omega) \geq 0$  is the amplitude of the transform and  $\psi_0(\omega)$  is its real-valued phase, then

$$0 \leq A_0(\omega) = A_0(-\omega) \text{ and } \psi_0(-\omega) = -\psi_0(\omega). \quad (21)$$

The symmetry of  $A_0(\omega)$  guarantees that if  $\omega_0 > 0$  is a global maximum of  $A_0(\omega)$ , then so is  $-\omega_0$ . We will use both of these points next. We define the first residual  $R_1(\omega)$  by

$$R_1(\omega) = \bar{f}(\omega) - \frac{D_0 h_0(\omega)}{\left( \int_{-\infty}^{\infty} h_0(\omega) \bar{h}_0(\omega) d\omega \right)^{1/2}} \quad (22)$$

with

$$D_0 = \frac{\int_{-\infty}^{\infty} A_0(\omega) \exp(-j\psi_0(\omega)) \bar{h}_0(\omega) d\omega}{\left( \int_{-\infty}^{\infty} h_0(\omega) \bar{h}_0(\omega) d\omega \right)^{1/2}} \quad (23)$$

and

$$h_0(\omega) = \frac{1}{(\pi\alpha_0)^{1/4}} \left( \exp\left( \frac{-(\omega - \omega_0)^2}{2\alpha_0} \right) \right. \\ \left. - j \left( \psi_0 + t_0(\omega - \omega_0) + \frac{\kappa_0}{2}(\omega - \omega_0)^2 \right) \right) \\ \left. + \exp\left( \frac{-(\omega + \omega_0)^2}{2\alpha_0} \right) + j \left( \psi_0 - t_0(\omega + \omega_0) \right. \right. \\ \left. \left. + \frac{\kappa_0}{2}(\omega + \omega_0)^2 \right) \right) \quad (24)$$

where  $\omega_0 > 0$  is the location of the positive global maximum of  $A_0(\omega)$ , the parameters  $(\psi_0, t_0, \kappa_0)$  are given by

$$\psi_0 = \psi_0(\omega_0), \quad t_0 = \psi_0^{(1)}(\omega_0), \quad \text{and } \kappa_0 = \psi_0^{(2)}(\omega_0) \quad (25)$$

and  $\alpha_0$  is chosen to maximize  $|D_0|$ .

The fact that  $A_0(\omega)$  and  $\psi_0(\omega)$  satisfy (21) along with the identity that  $\bar{h}_0(\omega) = h_0(-\omega)$  guarantees that  $D_0$  is real, that  $R_1(\omega)$  satisfies  $\bar{R}_1(\omega) = R_1(-\omega)$ , and that  $R_1(\omega)$  may be written as

$$R_1(\omega) = A_1(\omega) \exp(-j\psi_1(\omega)) \quad (26)$$

where  $A_1(\omega)$  and  $\psi_1(\omega)$  satisfy (21). The residual  $R_1(\omega)$  also satisfies

$$\int_{-\infty}^{\infty} A_1^2(\omega) d\omega = \int_{-\infty}^{\infty} A_0^2(\omega) d\omega - D_0^2. \quad (27)$$

One now proceeds inductively in going from the  $k$ th residual to the  $(k + 1)$ th. The key fact is that the  $k$ th residual  $R_k(\omega) = A_k(\omega) \exp(-j\psi_k(\omega))$  satisfies  $\bar{R}_k(\omega) = R_k(-\omega)$ . This guarantees that

$$0 \leq A_k(\omega) = A_k(-\omega) \text{ and } \psi_k(-\omega) = -\psi_k(\omega) \quad (28)$$

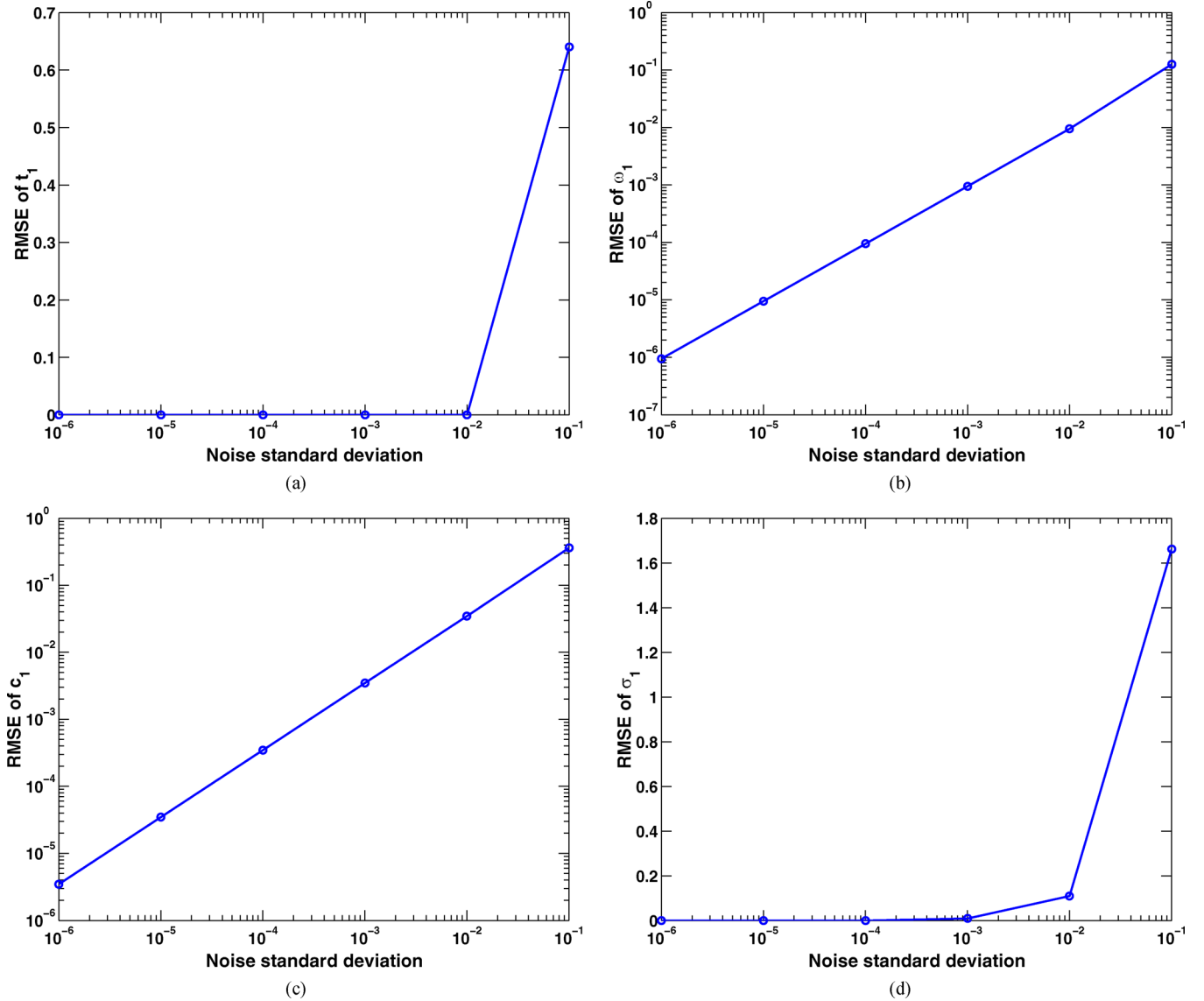


Fig. 1. Root mean-square errors (RMSEs) of  $t_1$ ,  $\omega_1$ ,  $c_1$ , and  $\sigma_1$  as functions of the noise standard deviation. The signal consists of one chirplet and additive complex Gaussian noise. (a) RMSE of  $t_1$ . (b) RMSE of  $\omega_1$ . (c) RMSE of  $c_1$ . (d) RMSE of  $\sigma_1$ .

and thus implies that if  $\omega_k > 0$  is the location of a global maximum of  $A_k(\omega)$  then so is  $-\omega_k$ . One then repeats (22)–(23) with the index 0 replaced by  $k$  and arrives at the formula for the  $(k + 1)$ th residual. One also has (27) with the index 0 replaced by  $k$  and 1 by  $k + 1$ . The identity that  $(k + 1)$ th residual in the time domain is given by

$$\begin{aligned} R_{k+1}(t) &\stackrel{\text{def}}{=} \frac{1}{2\pi} \int_{-\infty}^{\infty} \exp(j\omega t) R_{k+1}(\omega) d\omega \\ &= f(t) - \frac{1}{2\pi} \sum_{p=0}^k D_p \frac{\int_{-\infty}^{\infty} \exp(j\omega t) h_p(\omega) d\omega}{\left( \int_{-\infty}^{\infty} h_p(s) \bar{h}_p(s) ds \right)^{1/2}} \end{aligned} \quad (29)$$

and the identity (30), shown at the bottom of the next page, yields the chirplet expansion for the real-valued signal  $f(t)$ .

In addition to using the above frequency-domain algorithm for chirplet approximation, we can employ the time-domain algorithm

in Section II, provided that the real-valued signal is properly pre-processed. Specifically, in the preprocessing stage, we compute the complex-valued analytic signal of the real-valued signal based on the Hilbert transform. We then apply the time-domain algorithm and decompose the analytic signal into several chirplets. The sum of these chirplets and their complex conjugates constitute the approximation of the original real-valued signal.

#### IV. RECURSIVE CHIRPLET PARAMETER ESTIMATION

We can implement the algorithms in the previous sections for chirplet approximation in a direct sequential way. After the parameters of the first chirplet are estimated, the first chirplet is reconstructed and subtracted out from the original signal. Based on the remaining signal, the parameters of the second chirplet are estimated. Then, the second chirplet is reconstructed and subtracted out from the remaining signal. This process goes on until all the parameters of the existing chirplets have been estimated.

The problem with direct sequential estimation is that the estimation errors of the initial chirplets may significantly affect the estimation accuracy of the subsequent chirplets. To reduce such an error propagation effect, we consider recursive chirplet parameter estimation by exploiting a relaxation (RELAX)-based algorithm, which was originally proposed for estimating sinusoidal parameters in the presence of noise [7] and later was used for angle and waveform estimation [8]. The RELAX algorithm can be used in conjunction with either the time-domain algorithm or the frequency-domain algorithm to refine the chirplet parameter estimates.

We use the time-domain algorithm as an example to illustrate the steps of RELAX. Let  $K$  denote the number of chirplets we wish to estimate in the signal.

Define

$$Y_k(t) = R_0(t) - \sum_{i=0, i \neq k}^{K-1} \hat{C}_i g(t - \hat{t}_i; \hat{\sigma}_i, \hat{\omega}_i, \hat{c}_i) \quad (31)$$

where  $\{\hat{t}_i, \hat{\omega}_i, \hat{c}_i, \hat{\sigma}_i, \hat{C}_i\}_{i=0}^{K-1}$  are the estimated chirplet parameters.

The RELAX algorithm consists of the following steps.

- Step 1: Assume  $K = 1$ . Obtain  $\hat{t}_0, \hat{\omega}_0, \hat{c}_0, \hat{\sigma}_0$  and  $\hat{C}_0$  from  $R_0(t)$ .
- Step 2: Assume  $K = 2$ . Compute  $Y_1(t)$  with (31) by using  $\hat{t}_0, \hat{\omega}_0, \hat{c}_0, \hat{\sigma}_0$ , and  $\hat{C}_0$  obtained in Step 1. Obtain  $\hat{t}_1, \hat{\omega}_1, \hat{c}_1, \hat{\sigma}_1$ , and  $\hat{C}_1$  from  $Y_1(t)$ . Next, compute  $Y_0(t)$  with (31) by using  $\hat{t}_1, \hat{\omega}_1, \hat{c}_1, \hat{\sigma}_1$ , and  $\hat{C}_1$  and redetermine  $\hat{t}_0, \hat{\omega}_0, \hat{c}_0, \hat{\sigma}_0$ , and  $\hat{C}_0$  from  $Y_0(t)$ . Iterate the previous two substeps until “practical convergence” is achieved (to be discussed later on).
- Step 3: Assume  $K = 3$ . Compute  $Y_2(t)$  with (31) by using  $\{\hat{t}_i, \hat{\omega}_i, \hat{c}_i, \hat{\sigma}_i, \hat{C}_i\}_{i=0}^2$  obtained in Step 2. Obtain  $\hat{t}_2, \hat{\omega}_2, \hat{c}_2, \hat{\sigma}_2$  and  $\hat{C}_2$  from  $Y_2(t)$ . Next, compute  $Y_0(t)$  with (31) by using  $\{\hat{t}_i, \hat{\omega}_i, \hat{c}_i, \hat{\sigma}_i, \hat{C}_i\}_{i=1}^2$  and redetermine  $\hat{t}_0, \hat{\omega}_0, \hat{c}_0, \hat{\sigma}_0$ , and  $\hat{C}_0$  from  $Y_0(t)$ . Then, compute  $Y_1(t)$  with (31) by using  $\{\hat{t}_i, \hat{\omega}_i, \hat{c}_i, \hat{\sigma}_i, \hat{C}_i\}_{i=0,2}$  and redetermine  $\hat{t}_1, \hat{\omega}_1, \hat{c}_1, \hat{\sigma}_1$  and  $\hat{C}_1$  from  $Y_1(t)$ . Iterate the previous three substeps until “practical convergence.”
- Remaining Steps: Continue similarly until  $K$  is equal to the desired or estimated number of chirplets.

The “practical convergence” in the iterations of the RELAX algorithm may be determined by checking if the relative changes of the parameter estimates are sufficiently small or if a preset maximum number of iterations is reached.

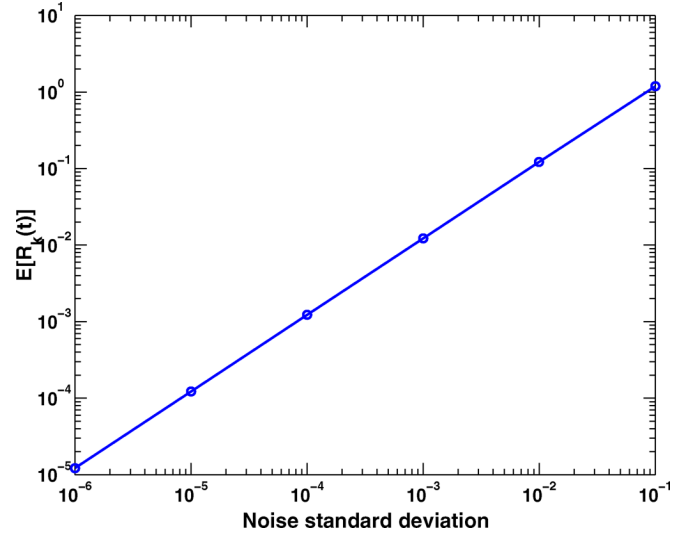


Fig. 2. Residue mean as a function of the noise standard deviation. The signal consists of one chirplet and additive complex Gaussian noise.

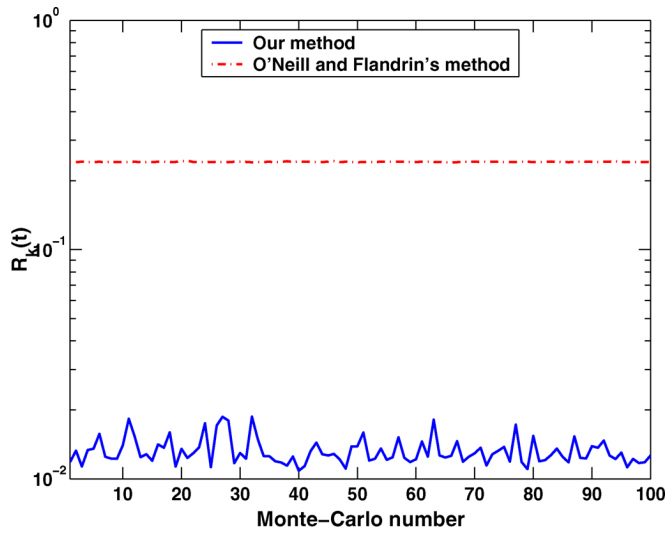
## V. NUMERICAL EXAMPLES

We provide several simulated examples to demonstrate the effectiveness of the chirplet approximation algorithms. In all of the examples considered below, we assume that the signal is a discrete time sequence of  $N = 128$  samples composed of several chirplets and additive zero-mean circularly symmetric complex Gaussian noise. Accordingly, we use difference and summation operations instead of differentiation and integration operations, respectively, in the algorithms. For complex-valued signals, we have proposed two time-domain algorithms. The first one is faster than the second one since it does not require a one-dimensional search for  $\sigma_k$ . However, numerical examples show that in the presence of noise or multiple chirplets, the estimates of  $\{\sigma_k\}$  obtained via the first algorithm are not as accurate as those obtained via the second. In the examples below, whenever we deal with chirplet approximation for complex-valued signals in the time domain, the second algorithm is used. We define the *residue* at the  $k$ th stage as the Euclidean norm of the remaining signal after  $k$  chirplets are reconstructed and subtracted out from the original signal.

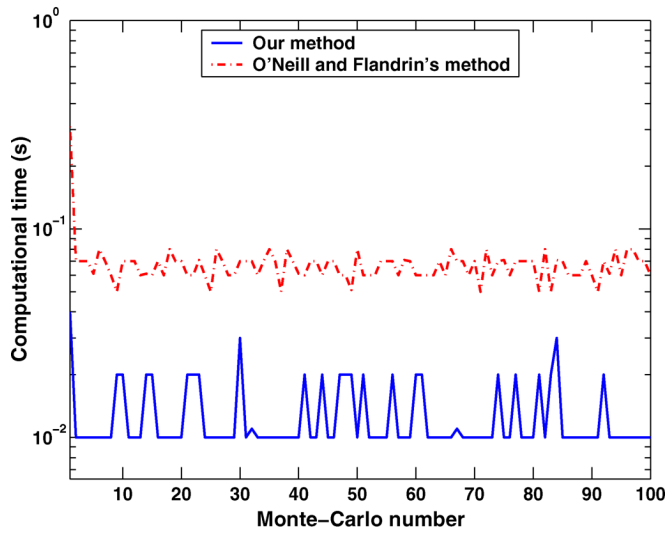
### A. Example 1

In the first example, we consider a signal consisting of one chirplet and additive complex Gaussian noise. The chirplet has the following parameters:  $C_1 \exp(-j\phi_1) = 1, t_1 = 54, \omega_1 = 40\pi/N, c_1 = 2\pi/N,$

$$\begin{aligned} & \int_{-\infty}^{\infty} \exp(j\omega t) h_p(\omega) d\omega \\ &= 2^{3/2} (\pi \alpha_p)^{1/4} \operatorname{Re} \left( \frac{\exp \left( \frac{-\alpha_p (t-t_p)^2}{2(1+\kappa_p^2 \alpha_p^2)} + j \left( (\psi_p - \omega_p t_p) - \omega_p (t-t_p) - \frac{\kappa_p \alpha_p^2 (t-t_p)^2}{2(1+\kappa_p^2 \alpha_p^2)} \right) \right)}{(1-j\kappa_p \alpha_p)^{1/2}} \right) \end{aligned} \quad (30)$$



(a)



(b)

Fig. 3. Comparison of our method and O'Neill and Flandrin's method in terms of (a) residue and (b) computational time. The signal consists of one chirplet and additive complex Gaussian noise.

and  $\sigma_1 = 4$ . We examine the effect of the noise standard deviation on the chirplet parameter estimates obtained from 100 Monte Carlo simulations. In Fig. 1(a)–(d), the root mean-square errors (RMSEs) of the chirplet parameters  $t_1$ ,  $\omega_1$ ,  $c_1$ , and  $\sigma_1$  are shown. The logarithm scale is not used in the  $y$  axis for Fig. 1(a) and (d) due to the fact that zero-valued RMSEs occur when the noise standard deviation is very small. As expected, the larger the noise standard deviation, the worse the parameter estimates. Fig. 2 shows the residue mean  $E[R_k(t)]$  as a function of the noise standard deviation after the estimated chirplet time sequence is subtracted out from the signal, where  $E[\cdot]$  denotes the expectation operator. Comparing Figs. 1 and 2, we see that the residue mean changes with respect to the noise standard deviation in a similar way as the RMSEs of the chirplet parameters. Hence, it can be used as a performance measure of the chirplet approximation. In Fig. 3, we compare the residue and computational time obtained via our method and O'Neill and Flandrin's method [3] for each of the above 100 Monte Carlo simulations when the noise standard deviation is equal to  $10^{-3}$ .

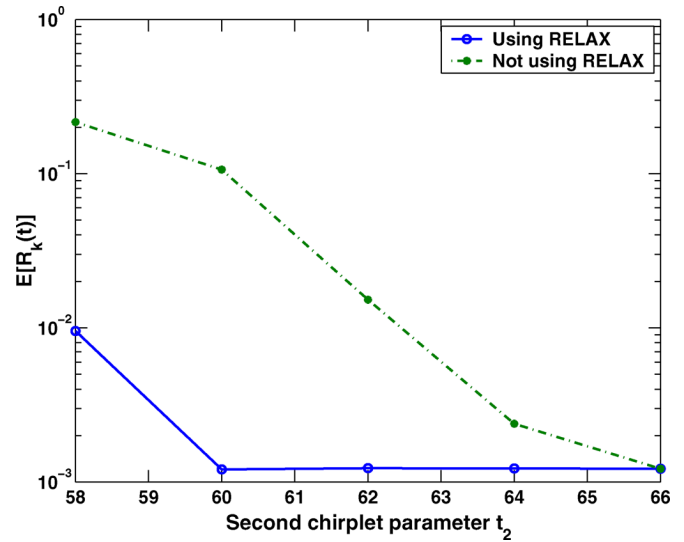


Fig. 4. Comparison of the residue means as functions of the second chirplet parameter  $t_2$ . The signal consists of two chirplets and additive complex Gaussian noise.

TABLE I  
PARAMETERS OF THE THREE CHIRPLETS IN THE THIRD EXAMPLE

$k$	$C_k \exp(-j\phi_k)$	$t_k$	$\omega_k$	$c_k$	$\sigma_k$
1	$\exp(-j\frac{8\pi}{N})$	64	$0.2\pi$	$\frac{3\pi}{N}$	10
2	$\exp(-j\frac{3\pi}{N})$	54	$0.1\pi$	$\frac{2\pi}{N}$	10
3	$\exp(-j\frac{10\pi}{N})$	74	$0.05\pi$	$\frac{\pi}{N}$	14

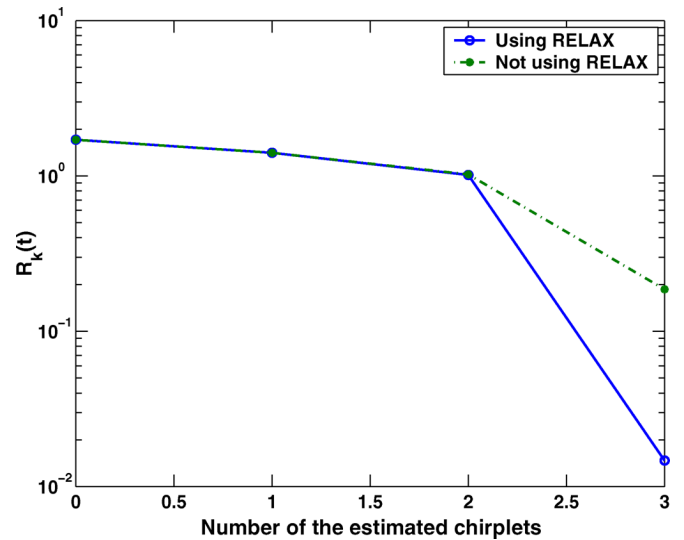


Fig. 5. Comparison of the residues as functions of the number of the estimated chirplets. The signal consists of three chirplets and additive complex Gaussian noise.

Neither method requires *a priori* complete dictionary of chirplets. The computational time measured in Matlab can indicate roughly the computational complexity of the chirplet decomposition. We see that our method not only requires less time than O'Neill and Flandrin's method but also has smaller residue than O'Neill and Flandrin's method.

TABLE II  
PARAMETER ESTIMATION ERRORS OF THE THREE CHIRPLETS IN THE  
THIRD EXAMPLE

$k$	Not using RELAX				Using RELAX			
	$t_k$	$\omega_k$	$c_k$	$\sigma_k$	$t_k$	$\omega_k$	$c_k$	$\sigma_k$
1	0	0.0042	0.0007	1.1900	0	0.0023	0.0005	0.1700
2	0	0.0187	0.0356	2.5000	0	0.0012	0.0031	0.0100
3	0	0.0051	0.0123	0.8400	0	0.0015	0.0001	0.2300

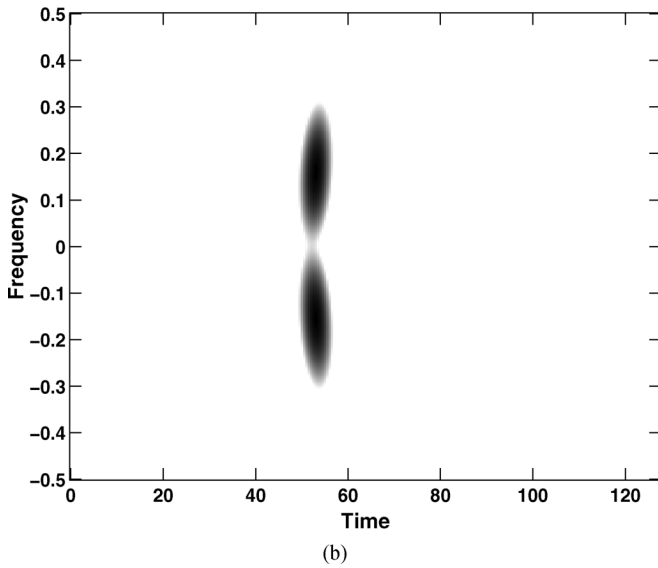
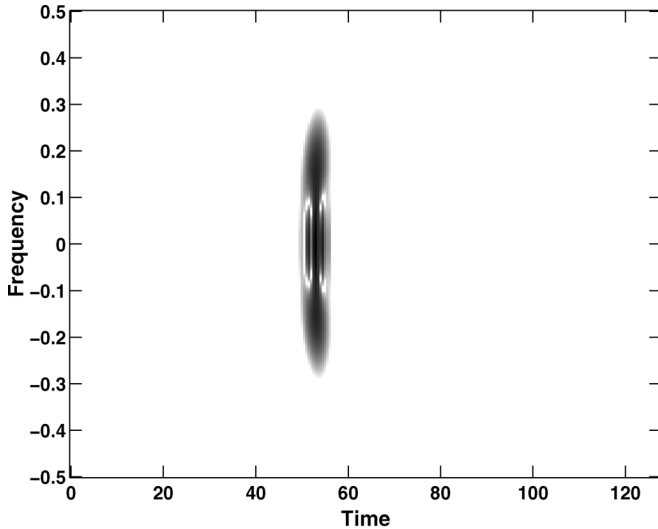


Fig. 6. (a) Wigner-Ville distribution of the real-valued signal, and (b) the sum of the Wigner-Ville distributions of the estimated pair of complex conjugate chirplets. Chirplet approximation is done in the frequency domain.

### B. Example 2

We consider in the second example a signal consisting of two chirplets and additive complex Gaussian noise. The first chirplet has the following parameters:  $C_1 \exp(-j\phi_1) = \exp(-j5\pi/N)$ ,  $t_1 = 54$ ,  $\omega_1 = 0.2\pi$ ,  $c_1 = 3\pi/N$ , and  $\sigma_1 = 3$ . The second chirplet has the same parameters as the first one except for  $t_2$ . In Fig. 4, we compare the residue means obtained via two methods as functions of  $t_2$  obtained

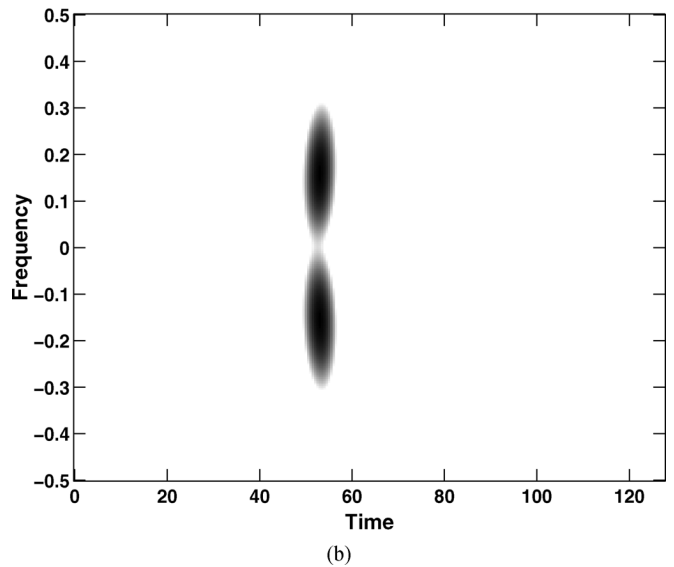
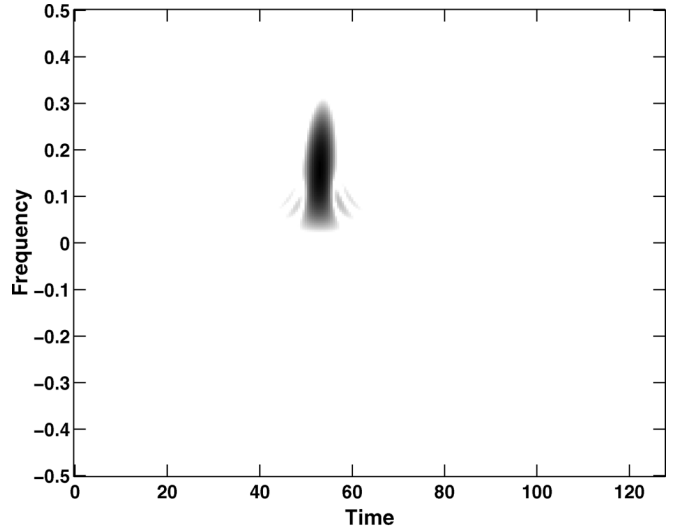


Fig. 7. (a) Wigner-Ville distribution of the analytic signal, and (b) the sum of the Wigner-Ville distributions of the estimated pair of complex conjugate chirplets. Chirplet approximation is done in the time domain.

via 100 Monte Carlo simulations with the noise standard deviation equal to  $10^{-4}$ . For the first method, we estimate the parameters of one chirplet first, subtract it out from the signal, and then estimate the parameters of the second chirplet. For the second method, we apply the RELAX based recursive algorithm by using cyclic chirplet approximation iterations to refine the parameter estimates. Fig. 4 demonstrates that RELAX can help reduce the residue significantly and hence improve the accuracy of the parameter estimates.

### C. Example 3

In the third example, we consider a signal consisting of three chirplets and additive complex Gaussian noise. The parameters of the three chirplets are shown in Table I. The noise standard deviation is equal to  $10^{-3}$  and we only use one realization of it. In Fig. 5, we compare the residues of these two methods as functions of the number of the estimated chirplets. The absolute values of the parameter

estimation errors of the two methods are listed in Table II. It is worth noting that RELAX can contribute to smaller residues and more accurate parameter estimates.

#### D. Example 4

Finally, we consider in the fourth example a real-valued signal, which is obtained by taking the real part of one realization of the signal in the first example with the noise standard deviation equal to  $10^{-4}$ . Fig. 6(a) shows the Wigner–Ville distribution of the real-valued signal. The artifacts near the zero frequency is due to the cross-term interferences of the Wigner–Ville distribution. To determine the parameters of the real-valued signal, we can explore two options. One way is to first use discrete Fourier transform (DFT) to transform the signal into the frequency domain and then use the frequency-domain chirplet approximation algorithm. Note that a pair of complex conjugate chirplet should be used as the bases. An alternative way for the chirplet approximation of the real-valued signal is to first compute its complex-valued analytic signal based on the Hilbert transform. Then, we can apply the time-domain chirplet approximation algorithm to the analytic signal to determine the corresponding chirplet. After that its complex conjugate counterpart can be obtained easily. Fig. 6(b) shows the sum of the Wigner–Ville distributions of the reconstructed pair of chirplets obtained via the first method. Fig. 7(a) shows the Wigner–Ville distribution of the analytic signal. Fig. 7(b) shows the sum of the Wigner–Ville distributions of the reconstructed pair of chirplets obtained via the second method. Note from Figs. 7(b) and 6(b) that the time-frequency distribution of the real-valued signal is readily observable and the artifacts near the zero frequency are eliminated. This demonstrates that both approaches can be used to estimate the chirplet parameters for a real-valued signal.

## VI. CONCLUSION

We have presented several time- and frequency-domain algorithms for efficient chirplet approximation of complex-valued and real-valued signals. We have also shown how a recursive relaxation (RELAX) based procedure can be used in conjunction with either the time-domain algorithm or the frequency-domain algorithm to improve the parameter estimation accuracy for multiple chirplets. Unlike previous methods, our chirplet approximations do not require any *a priori* complete dictionary of chirplets and complicated multidimensional searches to obtain suitable choices of chirplet parameters. Simulation results have demonstrated the effectiveness of the proposed approaches.

## REFERENCES

- [1] S. Mann and S. Haykin, "The chirplet transform: Physical considerations," *IEEE Trans. Signal Process.*, vol. 43, no. 11, pp. 2745–2761, Nov. 1995.
- [2] S. Mallat and Z. Zhang, "Matching pursuits with time-frequency dictionaries," *IEEE Trans. Signal Process.*, vol. 41, no. 12, pp. 3397–3415, Dec. 1993.
- [3] J. C. O'Neill and P. Flandrin, "Chirp hunting," in *Proc. IEEE Int. Symp. Time-Frequency Time-Scale Anal.*, Oct. 1998, pp. 425–428.
- [4] A. Bultan, "A four-parameter atomic decomposition of chirplets," *IEEE Trans. Signal Process.*, vol. 47, no. 3, pp. 731–745, Mar. 1999.
- [5] R. Gribonval, "Fast ridge pursuit with multiscale dictionary of gaussian chirps," *IEEE Trans. Signal Process.*, vol. 49, no. 5, pp. 994–1001, May 2001.
- [6] H. Kwok and D. Jones, "Improved FM demodulation in a fading environment," in *Proc. 3rd Int. Symp. Time-Frequency Time-Scale Anal. (TFTS-96)*, Paris, France, Feb. 1996, pp. 9–12.
- [7] J. Li and P. Stoica, "Efficient mixed-spectrum estimation with applications to target feature extraction," *IEEE Trans. Signal Process.*, vol. 44, no. 2, pp. 281–295, Feb. 1996.
- [8] J. Li, D. Zheng, and P. Stoica, "Angle and waveform estimation via RELAX," *IEEE Trans. Aerosp. Electron. Syst.*, vol. 33, pp. 1077–1087, Jul. 1997.